Magnetic properties of Gd_2O_3†

R. M. Moon and W. C. Koehler
Solid State Division, Oak Ridge National Laboratory, Oak Ridge, Tennessee 37830
(Received 22 August 1974)

Polarized-neutron experiments have been used to measure the temperature dependence of the susceptibility of the Gd^{3+} ion at the two different crystallographic sites in cubic Gd_2O_3 in the paramagnetic state. Below 10 °K these susceptibilities are quite different because of the different net exchange interactions with the rest of the crystal. The temperature dependences of the first- and second-neighbor spin correlations have also been observed through measurement of the diffuse scattering of unpolarized neutrons. An approximate theory of the magnetic behavior of Gd_2O_3 in the paramagnetic region is presented which provides predictions of the susceptibilities, spin correlations, and specific heat which are in reasonable accord with experimental results. The previously reported paramagnetic form factor for Gd_2O_3 has been revised slightly, leading to the conclusion that there is no convincing evidence supporting a difference in the $4f$ spin density between the metallic and oxide cases.

I. INTRODUCTION

In previous investigations[1,2] we measured the diffuse magnetic scattering of neutrons by cubic Gd_2O_3, thus obtaining a paramagnetic form factor. This form factor was slightly different than the $4f$ form factor for metallic Gd obtained from Bragg scattering of polarized neutrons.[2] Our original motivation in the present work was to check the Gd_2O_3 form factor using a different experimental technique. We would induce a net moment by application of a magnetic field at low temperatures, and then use the polarized-neutron technique to measure the magnetic structure factors of a number of Bragg peaks. Our first series of measurements of this type, carried out at 4.3 °K, indicated that the induced moments on Gd ions occupying different crystallographic sites were not equal, implying different ionic susceptibilities. In addition, we observed strong oscillations in the diffuse scattering, indicating short-range antiferromagnetic order. Our research goals were expanded to include studies of these two effects as functions of temperature. In this paper we present our experimental observations and an approximate theory of the behavior of Gd_2O_3 in the paramagnetic state. This theory not only gives good agreement with our results, but also is in reasonable agreement with conventional susceptibility and specific-heat observations.

One would expect Gd_2O_3 to have particularly simple magnetic properties, except perhaps at very low temperatures. In the Russell-Saunders coupling scheme, the Gd^{3+} ion has a $^8S_{7/2}$ ground state which should not be split by a crystalline electric field. Allowing for weak coupling between ions we expect Curie-Weiss paramagnetic behavior over a wide temperature range with the free-ion effective moment of $7.95\mu_B$. All this is certainly approximately true, as shown by the susceptibility measurements of Hacker, Lin, and Westrum,[3] but there are some interesting deviations from this ideal behavior. EPR spectra on the Gd^{3+} ion in a wide variety of crystalline environments show that the octet ground state is split by the crystal field. Typical splittings are of the order 0.3 °K. Buckmaster and Shing[4] have assembled a wealth of experimental data and have reviewed the unsatisfactory theoretical situation. The recent observation by Schinkel and Van Amstel[5] that the saturation moment in Gd_2O_3 is $6.9\mu_B$ rather than the expected value of $7.0\mu_B$ may be associated with the crystal-field effect.

There is confusion in the literature regarding magnetic order in Gd_2O_3. Specific-heat measurements on Gd metal[6-8] showed anomalies at 1.6 and 3.5 °K which were shown to be caused by oxide impurities of unknown stoichiometry and phase (there being both cubic and monoclinic forms of Gd_2O_3). Justice and Westrum[9] measured the specific heat of cubic Gd_2O_3 above 10 °K and observed the high-temperature tail of an anomaly occurring at some lower temperature. They were able to fit their data on the assumption that it was a Schottky anomaly caused by an over-all splitting of the octet ground state of 13.7 °K. This seems highly improbable in view of the much lower splittings observed by EPR in other systems. We will show that the Justice and Westrum data are rather the result of magnetic interactions between Gd^{3+} ions. In an effort to understand the two peaks seen in the specific heat of Gd metal, Miller *et al.*[10] have measured the low-temperature susceptibility of both the cubic and monoclinic phases of Gd_2O_3 for both stoichiometric and substoichiometric compositions. They found a typical antiferromagnetic transition in the substoichiometric monoclinic phase at 3.4 °K, in good agreement with the high-temperature specific-heat peak. For the cubic phase, they found no evidence of magnetic ordering down to

1.2 °K, observing only a change in slope of $1/\chi$ vs T at 2.8 °K. This result is in good agreement with earlier work by Brown and Hubbard[11] on the cubic phase. Both sets of authors attribute this change of slope to a crystal-field Schottky anomaly.

However, there is definite evidence that long-range magnetic order does occur in the cubic phase. Child *et al.*[1] have observed neutron diffraction peaks below 1.6 °K, indicating a complex antiferromagnetic order, and Katila *et al.*[12] have observed a magnetic transition at 1.35 °K by Mössbauer measurements. Why do the susceptibility results, which are normally a good indicator of magnetic ordering, fail to give this indication for Gd_2O_3?

Gd_2O_3 has the bixbyite structure[13] (space group $Ia3\text{-}T_h^7$) with a lattice constant of 10.813 Å. There are 24 Gd^{3+} ions on sites with twofold rotational symmetry (C_2) and 8 Gd^{3+} ions on sites with threefold rotary inversion symmetry (C_{3i}). The C_2 sites have a single positional parameter $u = -0.0304 \pm 0.007$, and the 48 oxygen sites are at a general position $x = 0.3913 \pm 0.0013$, $y = 0.1512 \pm 0.0012$, $z = 0.3811 \pm 0.0015$. These numbers were originally determined at 300 °K,[2] and, in the course of the present investigation, have been confirmed at 4.2 °K. The Gd sites are on four interpenetrating cubic lattices which, if the u parameter were zero, would form a face-centered cubic structure. Further details, helpful in visualizing the structure, are given by Pauling and Shappell[13] and by Moon *et al.*[14]

II. EXPERIMENTAL DETAILS

The sample was the same as that used in an earlier study,[2] consisting of 4.3 g of $^{160}Gd_2O_3$ powder obtained from the Stable Isotopes Division of this Laboratory. The isotopic purity was 99.993% ^{160}Gd. The sample was heated in air to drive off CO_2 and H_2O and sealed in an aluminum cylinder in a helium atmosphere. No evidence for a phase other than bixbyite was found in the diffraction patterns.

The experiments were performed on the HB-1 spectrometer at the High Flux Isotope Reactor. This spectrometer can be operated either in a polarized mode (Co-Fe monochromator) or an unpolarized mode (Be monochromator). The sample was mounted in the gap of a split-coil superconducting magnet providing a vertical field of up to 60 kOe and a $\frac{3}{4}$-in. gap in the scattering plane. Access to the center of the magnet is through a 1-in.-diam cylinder with a separate vacuum jacket running through the liquid helium reservior of the magnet. Controlled temperatures at the sample position can be obtained from 1.8 to 400 °K. No depolarization of the neutron beam is produced by the magnetic field configuration except when the magnet is operated at a very low central field.

In the polarized beam experiments we followed the standard technique[15] of measuring the ratio of Bragg intensities when the neutrons are polarized parallel, and then antiparallel, to the sample magnetization. Working with a fine-grained powder has the advantage that extinction and simultaneous reflection effects are negligible, in contrast to the single-crystal case. However, there is a counterpart of these effects in powder samples. Because the total Bragg scattering is dependent on the incident polarization, the sample transmission is dependent on the polarization. The magnitude of this effect is easily measured, and calculated corrections for cylindrical samples can be made with confidence. In our case, these corrections to the observed intensity ratios were about 1 percent. A more troublesome effect, and one unique to paramagnetic powders, was the unusual dependence of depolarization of the beam upon the applied field. Shown in Table I is the field dependence of the transmitted polarization ratio, measured on a Co-Fe analyzer placed after the sample. We believe the effect is caused by depolarization within the interparticle region of the sample. Field components perpendicular to the applied field will exist in these regions and their magnitudes will be proportional to the induced magnetization or applied field. Clearly, low fields are desirable to minimize depolarization, but the signal increases linearly with the field, so a compromise must be reached. Most of our data were obtained with a field of 18 kOe.

III. RESULTS

A. Polarized-beam experiments

In the polarized-beam experiments, we measured the ratio of intensities in Bragg peaks for neutrons polarized parallel and antiparallel to the applied field. For a centrosymmetric structure, this flipping ratio for a Bragg peak at the reciprocal lattice position $\vec{\tau}$ can be written as

$$R_\tau = [(1+\gamma_\tau)/(1-\gamma_\tau)]^2 , \tag{3.1}$$

where γ_τ is the ratio of the magnetic to the nuclear structure factor,

$$\gamma_\tau = F_\tau^M / F_\tau^N . \tag{3.2}$$

TABLE I. Polarization ratio transmitted through Gd_2O_3 at 4.3°K.

Field (kOe)	Ratio
12.5	77
25.0	35
50.0	12

TABLE II. Some geometric and nuclear structure factors for Gd_2O_3.

(hkl)	G_1	G_2	G_3	F^N	$\lvert F^N \rvert^2$
(211)	0.0	2.982	3.136	4.549	20.70
(220)	8.0	− 8.0	− 1.199	−0.696	0.48
(222)	−8.0	−22.270	− 0.242	−27.837	774.91
(231)	0.0	2.983	−10.162	−3.169	10.04
(321)	0.0	−2.983	13.446	5.075	25.75
(341)	0.0	−5.535	−4.018	−7.396	54.70
(431)	0.0	5.535	0.606	5.416	29.34
(440)	8.0	19.553	38.618	47.625	2268.12
(352)	0.0	2.983	3.599	4.818	23.21
(532)	0.0	−2.983	−6.264	−6.365	40.51
(611)	0.0	7.289	0.583	7.008	49.11
(622)	−8.0	−18.143	0.676	−23.529	553.59

For Gd_2O_3 we can write the nuclear structure factor as

$$F_\tau^N = \sum_{\nu=1} b_\nu G_\nu(\vec{\tau}) \exp[-B_\nu(\sin\theta/\lambda)^2] , \tag{3.3}$$

where $\nu = 1$ refers to the 8 Gd sites with C_{3i} symmetry, $\nu = 2$ refers to the 24 Gd sites with C_2 symmetry, $\nu = 3$ refers to the 48 oxygen sites, b_ν are the nuclear scattering amplitudes, and we have assumed an isotropic Debye-Waller factor B_ν for each set of sites. The geometric structure factor $G_\nu(\vec{\tau})$ is given by

$$G_\nu(\vec{\tau}) = \sum_j e^{i\vec{\tau}\cdot\vec{r}_{\nu j}} , \tag{3.4}$$

where the summation goes over all the positions $\vec{r}_{\nu j}$ of the set designated by ν. In an applied field a time-averaged magnetic moment is associated with each site, directed parallel to the applied field. The magnetic structure factor is

$$F_\tau^M = 0.2696\times10^{-12} \sum_{\nu=1} \mu_\nu f_\nu(\vec{\tau})\, G_\nu(\vec{\tau}) \times \exp[-B_\nu(\sin\theta/\lambda)^2] , \tag{3.5}$$

where μ_ν is the moment in Bohr magnetons associated with each site and $f_\nu(\vec{\tau})$ is the magnetic form factor for that site.

To use Eq. (3.2) for conversion of measured values of γ_τ into magnetic structure factors requires the calculation of nuclear structure factors using Eqs. (3.3) and (3.4). There are four positional parameters, two nuclear scattering amplitudes, and three temperature factors required to make this calculation, so it is clear that the interpretation of our results is not quite as clean as in the case of a simple structure with one kind of atom. At low temperatures we assume $B_\nu \ll 1$, and for relatively low scattering angles we have $(\sin\theta/\lambda)^2 \ll 1$, so that is a very good approximation to set the exponential factors in Eqs. (3.3) and (3.5) equal to unity. We neglect the small crystal-field effects on the Gd ions and assume that the ground state is that of a free ion in a magnetic field. The form factors on both Gd sites should then be the same and should be independent of field and temperature. The moments on the two sites may be different because of different magnetic interactions with the rest of the crystal. The oxygen moment is undoubtedly small and may be zero. With the approximations discussed above, Eq. (3.2) can be written as

$$\gamma_\tau F_\tau^N/0.2696 = [\mu_1 G_1(\tau) + \mu_2 G_2(\tau)] f_{\mathrm{Gd}}(\tau) + \mu_3 G_3(\tau) f_0(\tau) , \tag{3.6}$$

where F_τ^M is in units of 10^{-12} cm. The geometric structure factors and the total nuclear structure factor for a number of peaks are tabulated in Table II. We have used the position parameters given in Sec. I and nuclear amplitudes of 0.5803×10^{-12} cm for oxygen and 0.915×10^{-12} cm for Gd in calculating these numbers. Inspection of Table II shows that some peaks, like the (222), have a total magnetic contribution very closely proportional to the average Gd moment, while others, like the (211), do not depend on the moment on C_{3i} sites. Of particular interest is the (220) case which should have no magnetic contribution if the two Gd moments are equal and if there is no oxygen moment. Unfortunately, the (220) intensity (proportional to $\lvert F^N \rvert^2$ in zero field) is so weak that it may be nonobservable.

Our first experiments were a series of angular scans at 4.3 °K at various applied fields (0, 12.5, 25, and 50 kOe). We discovered the depolarization effect mentioned earlier during these experiments, established that we could adequately correct the data for this effect, and verified that the magnetic structure factors were varying linearly with the applied field. The 25-kOe scan is shown in Fig. 1. Note that the (220) peak, though very small, is definitely visible above the background. At zero applied field the (220) peak could not be detected. This immediately indicated that there was a magnetic contribution to the (220) and, therefore, that the Gd moments induced on the two sites were different and/or there was an induced moment on the oxygen sites.

Despite a very poor signal to background ratio, we were able to measure the (220) flipping ratio as 0.44 ± 0.06 in a field of 50 kOe. From the magnitude of the intensity we knew that $\lvert\gamma_{220}\rvert > 1$, and could then conclude that the magnetic structure factor had a value of $+3.4\pm10^{-12}$ cm. To account for this observation solely on the basis of a moment on the oxygen sites requires the ridiculous conclusion that there is at least $10\mu_B$ on each oxygen site directed opposite to the applied field! Thus, the conclusion is inescapable that the moments on the two Gd sites are different.

To establish the magnitude of a possible oxygen moment is difficult because there is no Bragg peak

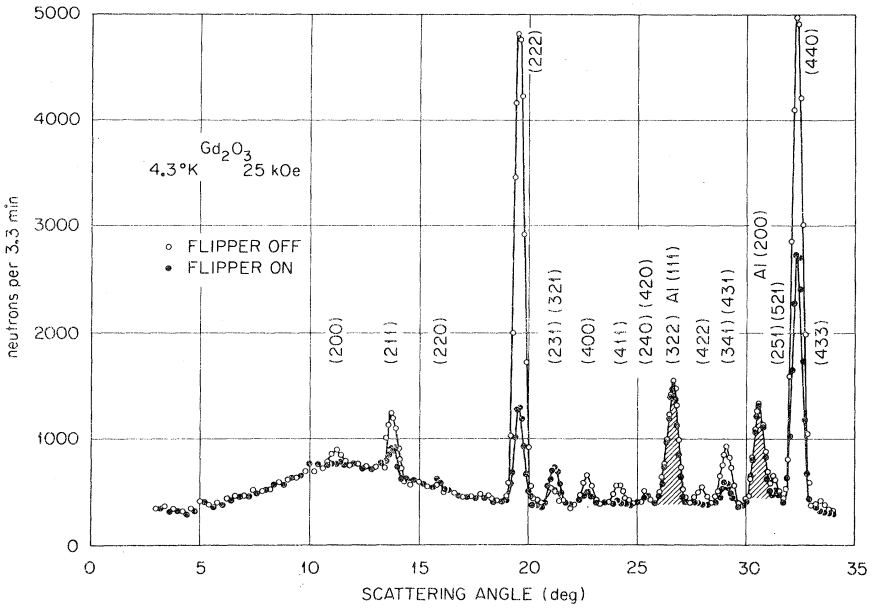

FIG. 1. Polarized-beam diffraction pattern for Gd_2O_3 powder at 4.3°K and 25 kOe. Neutron wavelength is 1.07 Å. Aluminum lines are from sample holder and cryostat.

which is sensitive to only an oxygen contribution. We measured flipping ratios on a number of peaks at 4.3 °K and 18 kOe and have performed a least-squares fit to these data, using the two Gd moments and an oxygen moment as variables. We used the Freeman-Desclaux[16] form factor for the Gd^{3+} ion and an estimated free-ion O^{2-} form factor. We do not expect a possible spin distribution on the oxygen sites to have the same shape as a free-ion charge density, but all we are really concerned with is any indication that the oxygen moment is not zero. The results of this fitting procedure are shown in Table III. The agreement between observed and calculated flipping ratios is satisfactory and the oxygen moment is zero within the indicated error. This experiment indicates that the oxygen contribution to the susceptibility is less than 2% of the total. In all that follows, we assume that the oxygen contribution is zero.

If the oxygen moment is negligibly small, the two Gd moments can be determined by observation of flipping ratios on only two peaks. We have studied the temperature dependence of the (211) and (222) peaks in a field of 18 kOe. Recall that the (211) depends only on the moment on the C_2 sites and the (222) depends on the moments on both sites. The raw flipping ratio data are shown in Fig. 2. Below 10 °K the two peaks have dramatically different temperature dependences. From these data we have deduced the ionic susceptibilities on the two Gd sites. After small corrections to the observed flipping ratios to account for instrumental effects, depolarization in the sample and the polarization dependence of the transmission, values of γ for each peak were obtained using Eq. (3.1). From Eq. (3.6) and Table II, we have

$$\mu_2 = (6.077 \pm 0.182)\gamma_{211}\,, \tag{3.7}$$

where the indicated error was obtained by considering the uncertainties in the structural parameters and scattering amplitudes. We have used 0.931 ± 0.005 for the (211) Gd form factor. Since there was some ambiguity about the best form factor in the oxide case[2] we have here used the mean of the Hartree-Fock calculation by Blume, Freeman, and Watson[17] and the Dirac-Fock result by Freeman and Desclaux.[16] The error indicates the small spread between these two calculations. Again using Eq. (3.6) and Table II for the (222) peak, and substituting Eq. (3.7) for μ_2, we have

$$\mu_1 = (14.887 \pm 0.149)\gamma_{222} - (16.917 \pm 0.541)\gamma_{211}\,, \tag{3.8}$$

where we have used 0.867 ± 0.007 for the (222)

TABLE III. Comparison of observed and calculated flipping ratios after least-squares adjustment of moments.

(*hkl*)	$R_{obs.}$	$R_{calc.}$
(211)	1.855 ± 0.088	1.803
(222)	3.320 ± 0.031	3.301
(231) + (321)	0.536 ± 0.030	0.568
(341) + (431)	1.692 ± 0.064	1.809
(440)	1.653 ± 0.014	1.642
(352) + (532) + (611)	1.584 ± 0.065	1.574
(622)	2.296 ± 0.027	2.339
$\mu_1 = 1.867 \pm 0.132$	Gd (C_{3i})	
$\mu_2 = 0.895 \pm 0.047$	Gd (C_2)	
$\mu_3 = -0.003 \pm 0.017$	Oxygen	

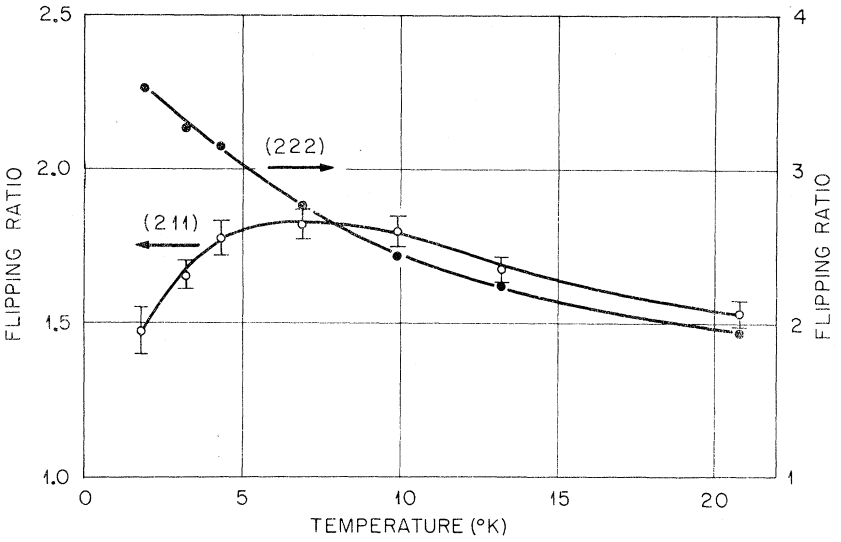

FIG. 2. Temperature dependencies of the (222) and (211) flipping ratios.

form factor. The average moment is given by

$$\bar{\mu} = \tfrac{1}{4}\mu_1 + \tfrac{3}{4}\mu_2$$
$$= (3.722 \pm 0.037)\gamma_{222} + (0.329 \pm 0.018)\gamma_{211} . \quad (3.9)$$

To calculate the susceptibilities corresponding to these moments, we need the internal field within a single particle of the powder sample, which is given in general by

$$\vec{H}_i = \vec{H}_0 - \vec{H}_D , \quad (3.10)$$

where $\vec{H}_0$ is the applied field and $\vec{H}_D$ is the demagnetizing field. We calculate an approximate value for $\vec{H}_D$ by considering a single spherical particle with magnetization $\vec{M}$, within a continuum with magnetization $\vec{M}f$, where f is the packing fraction of the powder sample. If D is the demagnetizing factor for the entire sample, we have

$$\vec{H}_D = 4\pi\vec{M}\left(\frac{1-f}{3} + Df\right) . \quad (3.11)$$

As shown by Bleaney and Hull[18] there is some experimental justification for this equation, but we are uncertain of its exact applicability to our sample, so we have allowed a 30% error in the calculated values of H_D. For our experiments H_D/H_0 varied from 0.03 to 0.06. The final susceptibilities are

$$\chi_i = \frac{N\mu_B\mu_i}{H_0 - H_D} , \quad (3.12)$$

where μ_i is given by Eq. (3.7), (3.8), or (3.9), μ_B is the Bohr magneton, and N is Avogardro's number. At 4.3 °K, the susceptibilities were independent of applied field up to 18 kOe, while at 1.8 °K the susceptibilities at 18 kOe were slightly smaller than at 6 and 12 kOe. The lower field strength data were used at this temperature.

The inverse susceptibilities are shown in Fig. 3 as a function of temperature. Above 10 °K there were no significant differences between χ_1 and χ_2,

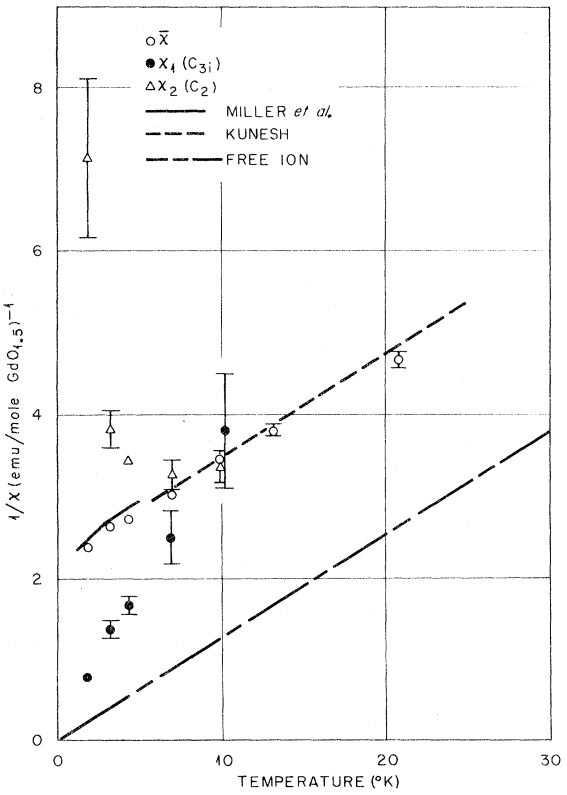

FIG. 3. Inverse susceptibilities of $GdO_{1.5}$ as a function of temperature. Data points are from polarized-beam measurements. Solid line is from Ref. 10. Dashed line is from measurements made at the University of Pittsburgh by C. J. Kunesh on a portion of our sample.

so only the average susceptibility is shown. Below 10 °K the two susceptibilities diverge quite rapidly and at 1.8 °K the susceptibility for the C_{3i} sites is larger than that for the C_2 sites by a factor of about 9. However, this divergence takes place in such a manner that nothing very striking happens to the average susceptibility, which is seen to be in good agreement with the ordinary susceptibility results. For complicated paramagnets, this kind of neutron experiment can clearly give more complete information than the ordinary susceptibility measurement. Similar experiments on Pr and Nd have been reported by Lebech and Rainford.[19]

Also shown in Fig. 3 is the calculated free-ion susceptibility for Gd^{3+}. The observed $1/\chi$ data are always higher than the free-ion result, indicating antiferromagnetic interactions between the Gd ions. A qualitative understanding of the bizarre behavior shown in Fig. 3 may be obtained by considering the possible effects of short-range magnetic order on the susceptibility. Suppose there is a strong tendency to form antiferromagnetic clusters of ions on C_2 sites, thus reducing the susceptibility of these ions. In considering the net interaction between one of these C_2 site clusters and an ion on a C_{3i} site, there will be a partial cancellation of individual pair interactions because of the antiferromagnetic nature of the cluster. As the C_2 sites get locked into an antiferromagnetic arrangement, the C_{3i} sites may become freer. At least this is the behavior suggested by Fig. 3. To understand better the nature of the spin correlations in Gd_2O_3 we next undertook a study of the diffuse scattering of neutrons as a function of temperature.

B. Diffuse scattering and spin correlations

The structure in the diffuse scattering at 4.3 °K is obvious in Fig. 1. This is evidence for short-range magnetic order, or nonzero correlation of spins on different sites. We wanted to study the temperature dependence of the spin correlations, not only to help in understanding the susceptibility results, but also because in our previous paramagnetic form-factor measurement we had assumed no correlation at 300 °K. In the present experiments, we measured the differential cross section, with no energy analysis, for unpolarized neutrons in zero magnetic field at temperatures ranging from 1.8 to 399 °K.

The basic correlation functions relevant to the magnetic scattering of neutrons are

$$\gamma_{\alpha\beta}(\vec{R}_l, t) = \frac{1}{N}\sum_m \langle S_m^\alpha(0) S_{m+l}^\beta(t)\rangle , \tag{3.13}$$

where S^α and S^β denote orthogonal components of the spin associated with sites at $\vec{R}_m$ at time zero and at $\vec{R}_m + \vec{R}_l$ at time t. The brackets denote a thermal average, and in our case the summation goes over all the Gd sites. These correlation functions are related to the double differential cross section (with respect to angle and final energy) as given by Marshall and Lovesey.[20] To relate the scattering theory to our experiment we must integrate the double differential cross section over the final energy. To do this integration we assume that the maximum possible energy transfer from magnetic interactions is very small compared to the incident neutron energy. This should be a good assumption in our case where the ordering temperature of Gd_2O_3 is 1.6 °K and we have used neutrons with kinetic energy of 829 °K (1.07 Å). In this case the momentum transfer at fixed scattering angle becomes nearly independent of the energy transfer, and the integration over energy is readily performed to obtain

$$\frac{d\sigma}{d\Omega} = \left(\frac{\gamma e^2}{mc^2}\right)^2 f^2(K) e^{-2W(K)} \sum_{\alpha\beta} (\delta_{\alpha\beta} - \hat{K}_\alpha \hat{K}_\beta) \times \sum_l e^{i\vec{K}\cdot\vec{R}_l} \gamma_{\alpha\beta}(\vec{R}_l, 0) . \tag{3.14}$$

We are here assuming the same isotropic form factor $f(K)$ and Debye-Waller factor $W(K)$ for all Gd ions. The summation goes over all vectors $\vec{R}_l$ connecting two Gd sites. Note that the correlation functions are evaluated at time zero, hence the name quasistatic approximation. This is essentially the x-ray limit, where an instantaneous picture of the sample configuration is obtained. We now assume that $\gamma_{\alpha\beta} = 0$ for $\alpha \neq \beta$, which is good for a Heisenberg interaction, and that $\gamma_{xx} = \gamma_{yy} = \gamma_{zz}$, which should be good for a cubic paramagnet. We define

$$\epsilon_l = \frac{\sum_m \langle \vec{S}_m(0) \cdot \vec{S}_{m+l}(0)\rangle}{NS(S+1)} , \tag{3.15}$$

so that

$$\gamma_{\alpha\beta}(\vec{R}_l, 0) = \tfrac{1}{3}\delta_{\alpha\beta} S(S+1)\epsilon_l . \tag{3.16}$$

Substituting Eq. (3.16) into Eq. (3.14) and performing a spherical integration for a powder sample, we obtain

$$\frac{d\sigma}{d\Omega} = \left(\frac{d\sigma}{d\Omega}\right)_p e^{-2W(K)} \sum_l \epsilon_l \frac{\sin KR_l}{KR_l} , \tag{3.17}$$

where the paramagnetic cross section for no correlation is given by

$$\left(\frac{d\sigma}{d\Omega}\right)_p = \frac{2}{3}\left(\frac{\gamma e^2}{mc^2}\right)^2 S(S+1) f^2(K) . \tag{3.18}$$

Note that the first term ($R_l = 0$) in the summation in Eq. (3.17) has the value of unity. The remaining terms are grouped according to common values of R_l in performing the sum, so that

$$\frac{d\sigma}{d\Omega} = \left(\frac{d\sigma}{d\Omega}\right)_p e^{-2W(K)} \left(1 + \sum_{l\neq 0} N_l \epsilon_l \frac{\sin KR_l}{KR_l}\right) , \tag{3.19}$$

where N_l is the number of Gd sites at a distance R_l from a fixed Gd site. So far we have not distinguished between the C_{3i} sites (type 1) and the C_2 sites (type 2). In fact, we believe that a 1-1 correlation may be quite different than a 2-2 correlation or a 1-2 correlation. If ${}^lN_{ij}$ is the number of type-j sites at a distance R_l from a type-i site and ${}^l\epsilon_{ij}$ is the spin correlation averaged over all i-j pairs at a distance R_l, then

$$N_l\bar{\epsilon}_l = \sum_{i,j=1}^{2} \omega_i\, {}^lN_{ij}\, {}^l\epsilon_{ij}\,, \tag{3.20}$$

where $\omega_1 = \frac{1}{4}$ and $\omega_2 = \frac{3}{4}$. Our goal is to attempt to fit the observed differential cross section with Eq. (3.19), using our knowledge of the structure to determine N_l and R_l with $\bar{\epsilon}_l$ as adjustable parameters. Only if the group of pairs defined by R_l involves a single combination of symmetry types will we be able to determine separate value for ${}^l\epsilon_{ij}$. Otherwise we must be content with the average correlation given in Eq. (3.20).

The essential details of the structure are given in Table IV. With data restricted to rather low values of K, it is clear from Eq. (3.19) that the fitting procedure cannot produce reliable numbers for values of R_l which are only slightly different. For example, it is hopeless to attempt to discriminate between the $l=1$ and $l=2$ shells of Table IV. We performed some fits with the $l=1$ and $l=2$ shells combined at their average distance and the $l=3$ and $l=4$ shells combined at their average distance. However, no significant difference in the correlations for these two distances were obtained. The final fitting procedure was based on the scheme shown on the right side of Table IV in which the first four shells are grouped together at a distance determined by the weighted mean of the individual values of R_l, with similar groupings made for the higher-order shells. The resulting coordination is the same as would be obtained if the u parameter were zero, but with slightly different values for the interatomic distances. Table IV was extended to $n=6$ in performing the least-squares fitting procedure. Applying Eq. (3.20) to the first two groups of shells, we see that

$$\bar{\epsilon}_1 = \tfrac{1}{2}\,{}^1\epsilon_{12} + \tfrac{1}{2}\,{}^1\epsilon_{22} \tag{3.21}$$

and

$$\bar{\epsilon}_2 = \tfrac{1}{4}\,{}^2\epsilon_{11} + \tfrac{3}{4}\,{}^2\epsilon_{22}\,. \tag{3.22}$$

The observed neutron diffuse intensity was converted to an absolute differential cross section by comparison with the integrated Bragg intensities. Unfortunately, the magnetic scattering which we have been considering is not the only source of diffuse scattering. The next most important source is multiple Bragg scattering, which should be approximately independent of temperature. To avoid making a calculated correction for the multiple Bragg scattering we have based our analysis on the observed difference in cross section at temperature T and at 300 °K. From Eq. (3.19) we have that

$$\left(\frac{d\sigma}{d\Omega}(T) - \frac{d\sigma}{d\Omega}(300)\right)\Big/\left(\frac{d\sigma}{d\Omega}\right)_p = \sum_{n\neq 0} N_n[\bar{\epsilon}_n(T) - \bar{\epsilon}_n(300)]\,\frac{\sin K\bar{R}_n}{K\bar{R}_n}\,. \tag{3.23}$$

Here we have neglected the Debye-Waller factor appearing in Eq. (3.19), and we have also neglected a small temperature-dependent contribution to the diffuse scattering due to phonons. Estimated corrections for these thermal effects, based on the very small temperature dependence observed for the Bragg peaks, were always considerably smaller than the statistical errors in the cross sections. The effect of thermal expansion, which produces a very slight temperature dependence in R_n, is negligible. For the denominator on the left-hand side of Eq. (3.23) we have used the previously determined[2] cross section at 300 °K. We could also have used a calculated cross section based on Eq. (3.18) without a significant effect on the results.

The left-hand side of Eq. (3.23) is thus completely determined experimentally. We attempted to fit the shape of these curves using values of N_n and $\bar{R}_n$ from Table IV. The comparison of the data and the calculated least-squares fit is shown in Fig. 4. The quality to the fit could be better at the two lowest temperatures, but the gross features of the data are well represented by the calculated curves. The curves shown are the result of a six-parameter fit, but only the first two correlation functions were significantly different from zero. The values for these first two correlations did not change significantly when the number of parameters was changed from six to three. Values for the first three correlations are given in Table V. Note that the first-

TABLE IV. Distribution of Gd–Gd pair distances in Gd_2O_3. ${}^lN_{ij}$ is the number of type j sites at a distance R_l from a type i site. $a = 10.813$ Å.

l	R_l/a	${}^lN_{11}$	${}^lN_{12}$	${}^lN_{21}$	${}^lN_{22}$	n	$\bar{R}_n/a$	N_n
1	0.3328	0	6	2	0			
2	0.3341	0	0	0	4			
3	0.3757	0	6	2	0			
4	0.3769	0	0	0	4	1	0.3549	12
5	0.5000	6	0	0	2			
6	0.5037	0	0	0	4	2	0.5018	6
7	0.5755	0	0	0	4			
8	0.6006	0	12	4	0			
9	0.6014	0	0	0	4			
10	0.6254	0	12	4	0			
11	0.6261	0	0	0	4			
12	0.6500	0	0	0	4	3	0.6131	24

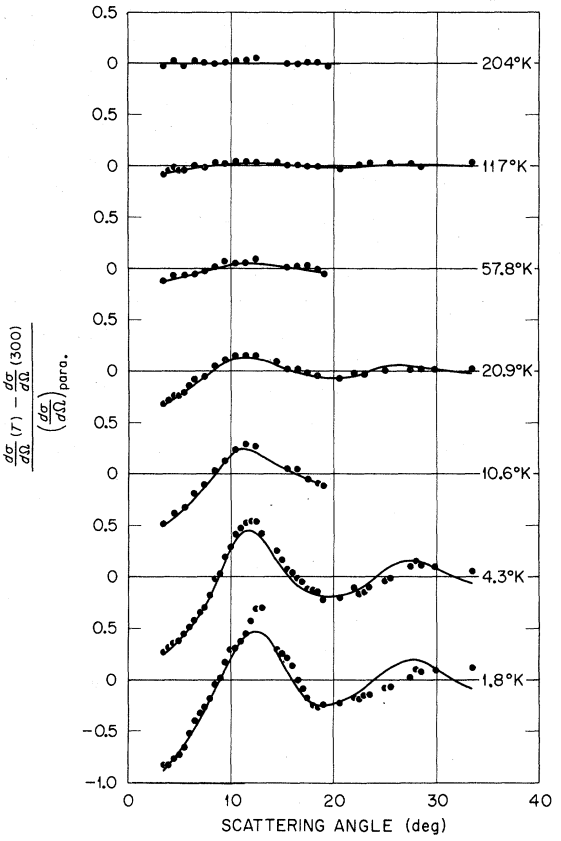

FIG. 4. Diffuse scattering data at various temperatures and zero applied field. Unpolarized neutrons of 1.07-Å wavelength were used. The solid lines are least-squares fits using the quasistatic approximation given in the text.

neighbor correlation is negative (antiferromagnetic) and the second-neighbor correlation is positive (ferromagnetic). One should not conclude that these results indicate that the range of the magnetic interaction extends at least to second neighbors. In this structure, second neighbors have four common first neighbors, so that a second-neighbor correlation can be produced by a propagation of first-neighbor correlations. In fact, you can predict quite accurately the second-neighbor correlations in Table V using the crude assumption that

$$\bar{\epsilon}_2 = 4\,\bar{\epsilon}_1^2 \,. \tag{3.24}$$

This indicates that the dominant magnetic interaction probably extends only to first neighbors. The data of Table V show that at 300 °K the rate of change of the first-neighbor correlation with respect to temperature is negligibly small, which is not the same thing as showing that the correlation itself is negligibly small. In a later section we will describe a model which successfully predicts the data shown in Table V. We can then use this model, with a high degree of confidence, to calculate the small correlation remaining at 300 °K.

C. Form factor

In the analysis of our previous data[2] on the diffuse scattering at 300 °K, the assumption was made that there were no spin correlations. A theoretical model which accurately predicts the data of Table V indicates that the first-neighbor correlation at 300 °K is − 0.0047. This led to a general reconsideration of the earlier analysis with the following results.

First of all, the correction for the calculated spin correlation led to a maximum increase in the form factor at very small values of $\sin\theta/\lambda$ of about 2%. Beyond $\sin\theta/\lambda = 0.1$, the correlation correction was generally smaller than the experimental error.

Secondly, a slightly different calibration constant was used to convert the observed intensities to absolute cross sections. In the earlier analysis this calibration was based on Bragg peaks from a silicon powder sample substituted for the Gd_2O_3 sample. In the present analysis an internal calibration using the (222) peak from Gd_2O_3 was employed. The two calibrations differ by only 1.6% in their effect on the form factor and have overlapping errors. The internal calibration is a cleaner technique because one does not have to determine the packing densities of the two samples, nor worry about placing the two samples exactly in the same position in the neutron beam. Furthermore, the (222) peak has a very small oxygen contribution and is rather insensitive to the Gd structural parameter, so its structure factor is primarily dependent on the Gd nuclear scattering amplitude. This is desirable for comparing the oxide form factor with the metallic form factor since the metallic data were measured relative to the same nuclear amplitude.

Finally, the original analysis did not include a correction for the thermal motion of the Gd ions, which we have tried to rectify in the present analysis. However, our knowledge of the proper mag-

TABLE V. Values of $[\bar{\epsilon}_n(T) - \bar{\epsilon}_n(300)]$ obtained from least-squares fits of diffuse scattering data.

T(°K)	$n=1$	$n=2$	$n=3$
1.8	−0.147(6)	+0.119(25)	+0.012(10)
4.3	−0.130(4)	+0.071(17)	+0.016(7)
10.6	−0.073(6)	+0.016(35)	+0.006(16)
20.9	−0.046(2)	+0.011(8)	+0.001(3)
57.8	−0.019(4)	+0.011(21)	−0.003(10)
117.0	−0.010(2)	−0.002(6)	+0.001(2)
204.0	−0.003(2)		
399.0	−0.001(1)		

nitude of this correction is rather imprecise. Based on the small temperature dependence of the (440) peak, we obtain an upper limit for the temperature dependence of the gadolinium thermal parameter, $B(300) - B(4.2) = 0.11 \pm 0.09$. In correcting the form factor we have used the value $B(300) = 0.15 \pm 0.15$, which should be an adequate expression of our uncertainty. The effect of this correction is to increase the outer data points slightly relative to the inner ones and to increase the errors in the outer points.

The revised paramagnetic form factor is shown as the open data points in Fig. 5. The solid curves are calculations by Freeman and Desclaux[16] (Dirac-Fock) and by Blume, Freeman, and Watson[17] (Hartree-Fock), augmented by a small contribution for core polarization. In comparing the metallic and oxide data, the first two metallic points should be disregarded because they are influenced by conduction electron polarization. The case for a difference between the metal and oxide data is not as convincing as in our previous work. In fact, we no longer believe that there is a real difference. Either of the calculated form factors fit the oxide data equally well, however, the Dirac-Fock results clearly gives a superior fit to the metallic data (the Dirac-Fock result for the neutral atom is even better).

Also shown in Fig. 5 are four points obtained from polarized beam measurements on Bragg peaks from Gd_2O_3 at 4.3 °K. In a simple material which has only one kind of magnetic atom, a measurement on a single Bragg peak combined with a magnetization or susceptibility measurement yields a normalized magnetic form factor for that peak. In Gd_2O_3 the susceptibility measures the average moment while each Bragg peak responds to a different linear combination of the two Gd moments, so there is a problem. We have largely avoided this problem by selecting peaks for the form-factor measurement which are mainly dependent on the average moment, with only a small sensitivity for the difference in the two moments. If we define

$$\delta = (\mu_1 - \mu_2)/\bar{\mu} \,, \tag{3.25}$$

where $\bar{\mu}$ is the average Gd moment, then Eq. (3.6) may be written as

$$f_{Gd}(\tau) = \frac{\gamma_\tau F_\tau^N}{(0.2696)\bar{\mu}\left[G_1 + G_2 + \frac{1}{4}\delta(3G_1 - G_2)\right]} \,, \tag{3.26}$$

where we have again assumed there is no oxygen moment. For the form-factor measurements, it is possible to select certain peaks for which $3G_1 \simeq G_2$, and δ can be determined approximately from measurements on other peaks. Each measured value γ_τ then yields a normalized form factor with little sensitivity to the difference between the two moments, provided an accurate value for $\bar{\mu}$ is available from susceptibility results. This requires duplication of field, temperature, sample composition, and packing density in two experimental arrangements. To avoid a highly speculative estimate of errors in all these factors we have selected $\bar{\mu}$ so that the (222) form factor is in agreement with the diffuse scattering data. The remaining Bragg form factors are seen to be in good agreement with the diffuse data, showing that the two experimental techniques give results related by a scale factor. The susceptibility at 4.2 °K required by the normalization of the Bragg data is 0.350 emu per mole of $GdO_{1.5}$. This is in terms of applied field rather than internal field. On this same basis, and on a portion of our sample, Kunesh[21] has measured a value of 0.328. Published values of the susceptibility are 0.353 by Miller *et al.*[10] and 0.364 by Brown and Hubbard.[11]

Our conclusion is that there is no convincing experimental evidence for a difference in the 4*f* spin density in Gd metal and Gd_2O_3, and that relativistic Dirac-Fock calculations for the neutral atom give an accurate description of the 4*f* spin density in the metal.

IV. THEORY

A. General remarks

In this section we present an approximate theory of the spin correlations, susceptibility, and specific heat of Gd_2O_3 and compare the theory with experimental results. As a first step we consider the probable form of the dominant magnetic interaction.

The ordering temperature of 1.6 °K is low enough to force the consideration of the dipole-dipole interaction. The minimum dipolar energy for a pair of Gd^{3+} ions at the first-neighbor separation is

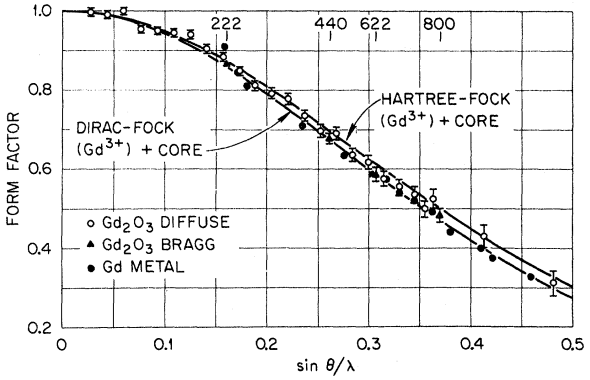

FIG. 5. Summary of Gd form factor measurements and calculations. The metallic data are from Ref. 2, the Dirac-Fock calculation is from Ref. 16, and the Hartree-Fock calculation is from Ref. 17.

$-1.1\,^{\circ}$K. This seems about the right order of magnitude, but there are two compelling reasons for rejecting the dipole-dipole interaction. It is basically a ferromagnetic interaction with a long range, whereas our experimental results indicate an antiferromagnetic interaction which extends only to first neighbors.

We will neglect the dipole-dipole interaction and assume superexchange interactions between first-neighbor gadolinium ions via their common oxygen neighbors. We represent this interaction for a specified pair by the usual Heisenberg Hamiltonian

$$H_{ex} = -2J_{ij}\vec{S}_i \cdot \vec{S}_j . \tag{4.1}$$

We can get an estimate of the average value of J_{ij} from the observed paramagnetic Curie temperature[3] of $-17\,^{\circ}$K. We obtain $J/k = -0.135\,^{\circ}$K, leading to a value for the minimum energy for a single pair of $-3.3\,^{\circ}$K. Negative values of J have the desired property of producing antiferromagnetic coupling.

We will simplify the structure by treating the case where $u = 0$, as we did in analyzing the experimental spin correlations. In this approximation the Gd ions fall on the sites of a cubic A_3B structure with a lattice constant half as large as the real lattice constant. The C_{3i} sites (type 1) are at the corners of the cube and the C_2 sites (type 2) are at the face-center positions. Some important features of this structure are set forth below.

(1) For a type-1 site, all twelve first neighbors are of type 2.

(2) For a type-2 site, four first neighbors are of type 1 and eight are of type 2.

(3) Each member of a 1-2 first-neighbor pair has four first neighbors of type 2 in common with the other member of the pair.

(4) Each member of a 2-2 pair has two first neighbors of type 2 and two first neighbors of type 1 in common with the other member of the pair.

The theory is based on the thermodynamics of an isolated pair of spins, with corrections to account approximately for the interactions with the rest of the crystal. The behavior of an isolated pair of spins coupled by a Heisenberg interaction is easy to calculate exactly. The thermodynamics can be given in terms of the spin correlation

$${}^0\epsilon_{ij}(J_{ij}/kT) \equiv \frac{\langle \vec{S}_i \cdot \vec{S}_j \rangle}{S(S+1)} , \tag{4.2}$$

which is readily calculated using the formulae or tables given by Smart.[22] Other thermodynamic quantities are easily obtained in terms of ${}^0\epsilon$. For example, the susceptibility of a collection of $N/2$ isolated pairs is

$${}^0\chi = \frac{Ng^2\mu_B^2 S(S+1)}{3kT}(1+{}^0\epsilon) = \frac{C}{T}(1+{}^0\epsilon) , \tag{4.3}$$

where C is the usual Curie constant.

Unfortunately, the Gd_2O_3 structure does not lend itself to direct application of the isolated pair theory. The existence of common first neighbors for each member of a pair is the principal difficulty. For antiferromagnetic interactions, this feature of the structure leads to competition between near-neighbor interactions and is the basic reason why the Néel point is so low compared to the paramagnetic Curie temperature.

B. Spin correlations

If two isolated ions have a spin correlation ϵ_{ij}, what is the change in this correlation when we bring a third ion in at position k to form an equilateral triangle? In first approximation, we assume that this change is given by the product $\epsilon_{ik}\epsilon_{kj}$. Bringing in additional ions would produce a change in ϵ_{ij} given by $\sum_k \epsilon_{ik}\epsilon_{kj}$. In this spirit, we write the first-neighbor correlations in Gd_2O_3 as

$${}^1\epsilon_{12} = {}^0\epsilon_{12} + 4\,{}^0\epsilon_{12}\,{}^1\epsilon_{22} \tag{4.4}$$

and

$${}^1\epsilon_{22} = {}^0\epsilon_{22} + 2\,{}^0\epsilon_{22}\,{}^1\epsilon_{22} + 2\,{}^0\epsilon_{12}\,{}^1\epsilon_{12} , \tag{4.5}$$

where ${}^0\epsilon_{ij}$ is the isolated pair correlation and can be calculated for a given J_{ij}. The coefficients and subscripts are dictated by the structure according to features (3) and (4) listed previously. The superscripts were chosen to give coupled linear equations in the unknown first-neighbor correlations ${}^1\epsilon_{ij}$. The neglect of higher-order correction terms limits the theory to the case of small correlations, with application to the paramagnetic state well above the ordering temperature. Note that for antiferromagnetic correlations ($\epsilon_{ij} < 0$), the quadratic terms provide a reduction in the magnitude of the isolated pair prediction, while the opposite is true for ferromagnetic correlations.

Solving for the ϵ_{ij}, we obtain

$${}^1\epsilon_{12} = ({}^0\epsilon_{12} + 2\,{}^0\epsilon_{12}\,{}^0\epsilon_{22})/D \tag{4.6}$$

and

$${}^1\epsilon_{22} = ({}^0\epsilon_{22} + 2\,{}^0\epsilon_{12}^2)/D , \tag{4.7}$$

where

$$D = 1 - 2\,{}^0\epsilon_{22} - 8\,{}^0\epsilon_{12}^2 . \tag{4.8}$$

To compare with the experimental results we need the average first-neighbor correlation given by Eq. (3.21),

$$\bar{\epsilon}_1 = ({}^0\epsilon_{12} + {}^0\epsilon_{22})(1 + 2\,{}^0\epsilon_{12})/2D . \tag{4.9}$$

To calculate the second-neighbor correlations we need some additional structural information. All second neighbors of a type-1 site are also type 1 and there are four first neighbors of type 2 com-

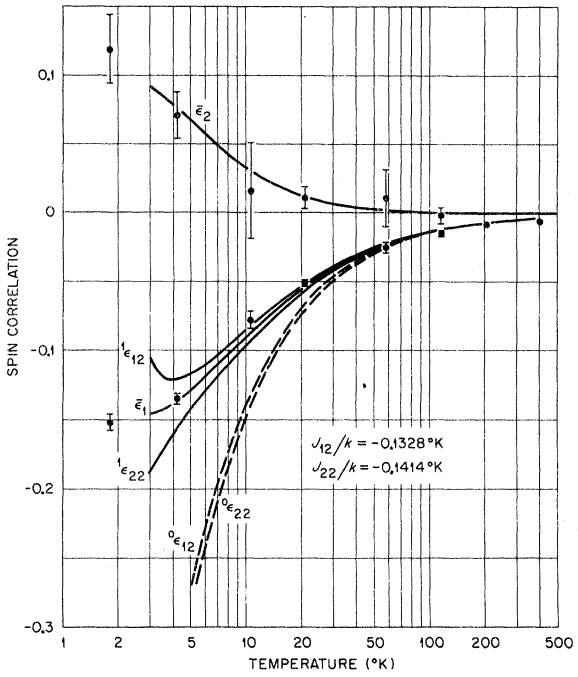

FIG. 6. Observed and calculated spin correlations in Gd_2O_3 as functions of temperature. The observed points should be compared with the curves labeled $\bar{\epsilon}_1$ and $\bar{\epsilon}_2$. The dashed lines show the prediction of the isolated pair theory for the indicated exchange interactions.

mon to both members of the pair. The 1-1 second-neighbor correlation thus is produced by four parallel 1-2-1 paths. We conclude that

$$^2\epsilon_{11} = 4\,{}^1\epsilon_{12}^2 . \tag{4.10}$$

All second neighbors of type 2 are also type 2; one third of these pairs have four common first neighbors of type 2, and two thirds of them have two common first neighbors of type 1 and two of type 2. We can write

$$^2\epsilon_{22} = \tfrac{4}{3}\,{}^1\epsilon_{12}^2 + \tfrac{8}{3}\,{}^1\epsilon_{22}^2 . \tag{4.11}$$

Using Eq. (3.22), we obtain for the average second-neighbor correlation,

$$\bar{\epsilon}_2 = 2({}^1\epsilon_{12}^2 + {}^1\epsilon_{22}^2) . \tag{4.12}$$

We are now able to calculate the temperature dependence of the average first- and second-neighbor correlations, given values for J_{12} and J_{22}. We have used $J_{12}/k = -0.1328$ °K and $J_{22}/k = -0.1414$ °K. These selections were made by fitting a further development of the theory to our susceptibility data at 5 °K. The comparison between theory and experiment is shown in Fig. 6 and is seen to be quite good. The calculated first-neighbor correlation at 300 °K is -0.0047, which has been added to the values given in Table V to obtain the experimental points in Fig. 6. It was expected that the theory would be satisfactory only for small correlations, so it is difficult to judge exactly which features of the calculation should be believed at low temperatures. Inspection of Eq. (4.6) shows that when $^0\epsilon_{22} = -0.5$, the theory predicts that $^1\epsilon_{12} = 0$. This is clearly nonphysical and occurs at about 2.5 °K for the calculation shown in Fig. 6. The calculated average correlations seem to be reasonable down to 3.0 °K, which suggests that the minimum in $^1\epsilon_{12}$ at about 4 °K might be real. If so, it would have a profound effect on the specific heat, as shown in the next section.

C. Specific heat

The total magnetic energy of the system in zero applied field is

$$E = -2\sum_{i<j} J_{ij}\langle \vec{S}_i \cdot \vec{S}_j \rangle$$
$$= -6NS(S+1)(J_{12}\,{}^1\epsilon_{12} + J_{22}\,{}^1\epsilon_{22}). \tag{4.13}$$

The electronic contribution to the specific heat is then given by

$$C_p = -6NS(S+1)\left(J_{12}\frac{\partial\,{}^1\epsilon_{12}}{\partial T} + J_{22}\frac{\partial\,{}^1\epsilon_{22}}{\partial T}\right). \tag{4.14}$$

We have performed a numerical differentiation of the calculated functions $^1\epsilon_{ij}$ to obtain the calculated specific heat shown in Fig. 7. The agreement with the observations of Justice and Westrum[9] would have been better if slightly larger values of J_{12} and J_{22} had been selected. On the other hand, the experimental points are subject to an unknown uncertainty involving the lattice contribution, so the agreement is probably satisfactory. Regardless of the validity of our model, the observed temperature dependence of the spin correlation requires a contribution to the specific heat like that observed by Justice and Westrum. It is not necessary to assume a low-temperature Schottky anomaly, as they did, to explain their data.

The calculated maximum in the specific heat, shown by the dashed line in Fig. 7, may not be

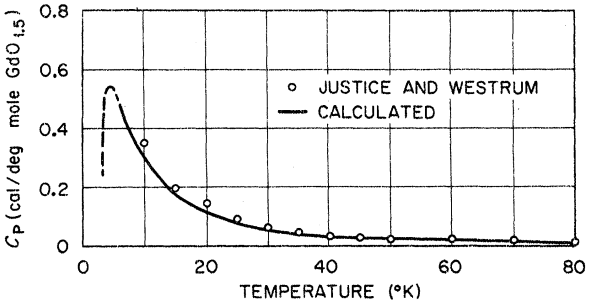

FIG. 7. Observed and calculated electronic specific heat for $GdO_{1.5}$. The dashed line shows an interesting but questionable prediction of our approximate theory.

real. Associated with the minimum of ${}^1\epsilon_{12}$, as shown in Fig. 6, it probably signals the breakdown of the theory at low temperature. We show it because of the remarkable agreement with one of the oxide-impurity peaks observed in the specific heat of Gd metal. If our calculated peak is real, then one can explain both of the impurity peaks assuming a single oxide phase. The 1.6 °K peak would be associated with long-range magnetic order in cubic Gd_2O_3 and the 3.5 °K peak would be associated with anomalous short-range order. If the calculated peak does not really exist, then one must assume that both the cubic and monoclinic oxides exist in the metallic samples, each ordering at a different temperature. Lounasmaa[8] has shown that his excess specific heat, observed on a metal of known oxygen content, joins smoothly with the Westrum and Justice data. This suggests a single phase for the oxide impurity in the metal, but is not conclusive. There seems to be no case in which the 1.6 °K peak was observed and the 3.5 °K peak was absent. Such a case would show that our calculated peak was fictitious. Dreyfus *et al.*[23] have made observations on a metallic sample in which only the 3.5 °K peak was observed, indicating that only the monoclinic impurity was present in their sample. The resolution of this question must await specific heat measurements on cubic Gd_2O_3 in the (1–10)°K range.

D. Susceptibility

The susceptibility calculation is based on the constant-coupling approximation,[24] adapted to the Gd_2O_3 structure. We treat a selected ion and one of its first neighbors as an isolated pair, and use an effective field approximation for the influence of the remaining first neighbors on the central ion. For a type-1 site, the moment induced by an internal field H_i is

$$M_1 = \chi_1 H_i = {}^0\chi_{12} H_i + 11\,\lambda_{12} M_2 , \tag{4.15}$$

where ${}^0\chi_{12}$ is the isolated pair susceptibility, given by Eq. (4.3), for a 1-2 pair and we have used the fact that all first neighbors of a type-1 site are of type 2. The parameter λ_{12} is closely related to the first-neighbor correlation, but for the moment we leave this relationship unspecified. Using the structural features discussed previously, the corresponding equation for the moment induced on a type-2 site is

$$M_2 = \chi_2 H_i = \tfrac{1}{3}({}^0\chi_{12} H_i + 3\,\lambda_{12} M_1 + 8\,\lambda_{22} M_2) + \tfrac{2}{3}({}^0\chi_{22} H_i + 4\,\lambda_{12} M_1 + 7\,\lambda_{22} M_2) . \tag{4.16}$$

Dividing both Eqs. (4.15) and (4.16) by H_i and solving for the susceptibilities, we obtain

$$\chi_1 = [(3 - 22\,\lambda_{22} + 11\,\lambda_{12})\,{}^0\chi_{12} + 22\,\lambda_{12}\,{}^0\chi_{22}]/B \tag{4.17}$$

and

$$\chi_2 = [(1 + 11\,\lambda_{12})\,{}^0\chi_{12} + 2\,{}^0\chi_{22}]/B, \tag{4.18}$$

where

$$B = 3 - 22\,\lambda_{22} - 121\,\lambda_{12}^2 . \tag{4.19}$$

Note that if ${}^0\chi_{12} = {}^0\chi_{22} = {}^0\chi$ and $\lambda_{12} = \lambda_{22} = \lambda$, then

$$\chi_1 = \chi_2 = \frac{{}^0\chi}{1 - 11\,\lambda} . \tag{4.20}$$

This is the usual constant-coupling equation for a system with 12 first neighbors if $\lambda = {}^0\epsilon$. This suggests that we set $\lambda_{ij} = {}^0\epsilon_{ij}$, but perhaps a choice more consistent with the theory of the zero-field correlations might be $\lambda_{ij} = {}^1\epsilon_{ij}$. Let us make a compromise choice,

$$\lambda_{ij} = b\,{}^0\epsilon_{ij} + (1 - b)\,{}^1\epsilon_{ij} , \tag{4.21}$$

and investigate the behavior of the average susceptibility in the high-temperature limit where it is known experimentally that the Curie-Weiss law is valid. In this region of very small correlations, we see from Eqs. (4.4) and (4.5) that ${}^1\epsilon_{ij} \to {}^0\epsilon_{ij}$, so that $\lambda_{ij} \to {}^0\epsilon_{ij}$. Using the known high-temperature behavior of ${}^0\epsilon_{ij}$,

$$\lim_{T\to\infty} {}^0\epsilon_{ij}(J_{ij}/kT) = \frac{2\,S(S+1)\,J_{ij}}{3kT} , \tag{4.22}$$

it follows from Eqs. (4.17) and (4.18) that

$$\lim_{T\to\infty} \bar{\chi} = \lim_{T\to\infty} (\tfrac{1}{4}\chi_1 + \tfrac{3}{4}\chi_2) = \frac{C}{T - \Theta} , \tag{4.23}$$

where

$$\Theta = \frac{2\,S(S+1)}{3k}\,(6\,J_{12} + 6\,J_{22}) \tag{4.24}$$

and C is the free-ion Curie constant given by Eq. (4.3). The theory gives the proper high-temperature behavior irrespective of the choice of b in Eq. (4.21). We have used $b = 0.5$ with experimental agreement as our only justification.

By combining the equations in this section with the previous calculation of the spin correlations, we can calculate the temperature dependence of χ_1, χ_2, and $\bar{\chi}$ with the two exchange parameters as the only adjustable input. The comparison with the neutron results is shown in Fig. 8 for the selected values of J_{12} and J_{22}. The simple theory does an adequate job of predicting rather complex behavior. Some feeling for the causes of the behavior shown in Fig. 8 can be obtained by inspecting Eqs. (4.15) and (4.16). The terms in ${}^0\chi_{ij}$, representing isolated pair susceptibilities, are positive and continuously increase as the temperature is decreased. The terms involving the λ_{ij} are negative and their

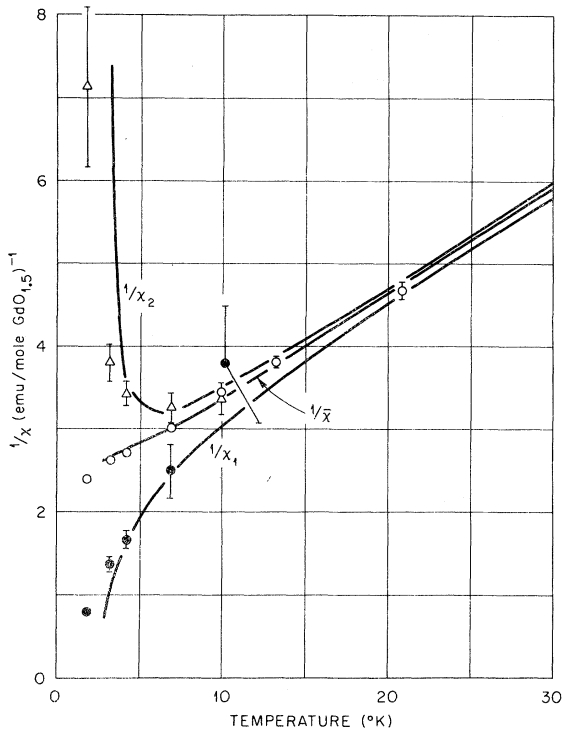

FIG. 8. Comparison of calculated susceptibilities with the polarized-beam results. The solid lines are calculated with $J_{12}/k = -0.1328$ °K and $J_{22}/k = -0.1414$ °K.

magnitude increases as the temperature is lowered. The increasing correlation, entering through the parameters λ_{ij}, opposes the normal thermal increase in the susceptibility as the temperature is lowered. For the type-2 sites, which have the strongest antiferromagnetic coupling with their neighbors, a temperature is reached where the correlation effect overcomes the thermal effect and the moment starts decreasing as the temperature is lowered. This tends to free the type-1 sites and they show a rapid increase in moment as soon as M_2 begins to decrease. This diverging behavior is nearly invisible if one looks at only the average susceptibility.

It is also of interest to compare the calculation of the average susceptibility with the results of ordinary susceptibility measurements. As shown in Fig. 9, the calculation shows Curie-Weiss behavior above 10 °K with a region of slight positive curvature in $1/\chi$ vs T from 3.5 °K to 10 °K. At 3.5 °K there is an abrupt change in slope similar to that seen experimentally at a somewhat lower temperature by Miller *et al.*[10] and by Brown and Hubbard.[11] Unfortunately this is in the temperature region in which the calculation is of uncertain validity because the correlations are becoming large. The region of positive curvature is not evident in any of the published data, but careful measurements in the right temperature range have not yet appeared. Probably such behavior has been seen by Schinkel and Van Amstel[5] because they report agreement with Miller *et al.* at low temperatures and Curie-Weiss behavior as shown in Fig. 9 above 20 °K. Miller *et al.* have shown that the low-temperature results depend strongly on the stoichiometry, so it is possible that some of the differences seen in Fig. 9 are sample dependent. The linear portion of the calculation can be translated vertically by adjusting the average exchange constant, but there seems to be no good reason to attempt this until the experimental results are more consistent with each other.

V. SUMMARY

The value of the polarized-neutron technique for investigating complicated paramagnets has been demonstrated. Whenever more than one type of magnetic atom is involved, a conventional susceptibility measurement gives only a partial description of the magnetic behavior because it measures the average response. As in the case of Gd_2O_3, the response of individual types of atoms may be quite different from the average and these differences can be resolved with the polarized-neutron technique.

The persistence of spin correlations at temperatures up to 100 times the ordering temperature has been demonstrated in Gd_2O_3, a material which has been regarded as nearly an ideal paramagnet. Such behavior suggests that diffuse scattering of neutrons from paramagnets is practically always affected by spin correlations to some degree and is therefore a poor method of obtaining form factor data, unless an independent study of the magnitude of the spin correlations is made. A reanalysis of our earlier measurement of the diffuse cross sec-

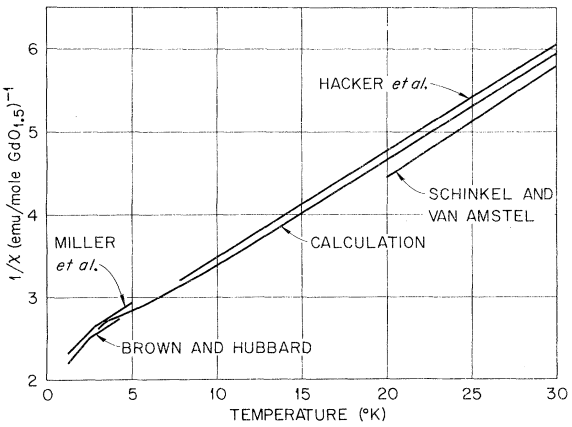

FIG. 9. Comparison of calculated average susceptibility with various experimental results using conventional techniques. See Refs. 10, 11, 3, and 5.

tion of Gd_2O_3 at 300 °K leads to the conclusion that there is no convincing experimental evidence supporting a difference in the $4f$ form factor between Gd metal and Gd_2O_3.

A simple theory of the magnetic behavior of Gd_2O_3 in the paramagnetic state has been developed which recognizes the differences in the net exchange interaction at the two different crystallographic sites. Two exchange constants are introduced, one measuring the strength of the interaction between a C_{3i} site and a C_2 site (J_{12}), and the other between two C_2 sites (J_{22}). The spin correlations, susceptibilities, and specific heat are calculated as a function of temperature. Good agreement with experimental results is found for $J_{12}/k = -0.1328$ °K and $J_{22}/k = -0.1414$ °K. The anomalous behavior of the susceptibility and specific heat, attributed by others to a single-ion Schottky anomaly, is almost certainly due to magnetic interactions between Gd ions.

ACKNOWLEDGMENTS

We are indebted to C. J. Kunesh, K. Narasimhan, and W. E. Wallace of the University of Pittsburgh for performing susceptibility measurements on our sample and to J. Sellers for valuable technical assistance.

†Research sponsored by the U. S. Atomic Energy Commission under contract with the Union Carbide Corp.

[1]H. R. Child, R. M. Moon, L. J. Raubenheimer, and W. C. Koehler, J. Appl. Phys. 38, 1381 (1967).

[2]R. M. Moon, W. C. Koehler, J. W. Cable, and H. R. Child, Phys. Rev. B 5, 997 (1972).

[3]H. Hacker, Jr., M. S. Lin, and E. F. Westrum, Jr., in *Rare Earth Research—III*, edited by L. Eyring (Gordon & Breach, New York, 1965), p. 93.

[4]H. A. Buckmaster and Y. H. Shing, Phys. Status Solidi A 12, 325 (1972).

[5]C. J. Schinkel and W. D. Van Amstel, Phys. Lett. A 44, 467 (1973).

[6]N. Kurti and R. S. Safrata, Philos. Mag. 3, 780 (1958).

[7]L. T. Crane, J. Chem. Phys. 36, 10 (1962).

[8]O. V. Lounasmaa, Phys. Rev. 129, 2460 (1963).

[9]B. H. Justice and E. F. Westrum, Jr., J. Phys. Chem. 67, 345 (1963).

[10]A. E. Miller, F. J. Jelinek, K. A. Gschneidner, Jr., and B. C. Gerstein, J. Chem. Phys. 55, 2647 (1971).

[11]R. E. Brown and W. M. Hubbard, Proceedings of the Fifth Rare-Earth Research Conference, Ames, Iowa, 1965 (unpublished), Vol. 4, p. 31.

[12]T. E. Katila, V. K. Typpi, and E. R. Seidel, *Proceedings of the Twelfth International Conference on Low Temperature Physics*, edited by E. Kanda (Academic Press of Japan, Tokyo, 1971), p. 711.

[13]L. Pauling and M. D. Shappell, Z. Kristallogr. 75, 128 (1930).

[14]R. M. Moon, W. C. Koehler, H. R. Child, and L. J. Raubenheimer, Phys. Rev. 176, 722 (1968).

[15]R. Nathans, C. G. Shull, G. Shirane, and A. Andresen, J. Phys. Chem. Solids 10, 138 (1959).

[16]A. J. Freeman and J. P. Desclaux, Int. J. Magn. 3, 311 (1972).

[17]M. Blume, A. J. Freeman, and R. E. Watson, J. Chem. Phys. 37, 1245 (1962).

[18]B. Bleaney and R. A. Hull, Proc. R. Soc. Lond. A 178, 86 (1941).

[19]B. Lebech and B. D. Rainford, J. Phys. (Paris) C 32, 1-370 (1971).

[20]W. Marshall and S. W. Lovesey, *Theory of Thermal Neutron Scattering* (Oxford U. P., Oxford, 1971), Chap. 8.

[21]C. J. Kunesh (private communication).

[22]J. Samuel Smart, *Effective Field Theories of Magnetism* (Saunders, Philadelphia, Pa., 1966), p. 51 and Appendix II.

[23]B. Dreyfus, J. C. Michel, and D. Thoulouze, Phys. Lett. 24A, 457 (1967).

[24]R. J. Elliott, J. Chem. Phys. Solids 16, 165 (1960).